RSC Advances

ROYAL SOCIETY OF CHEMISTRY

www.rsc.org/advances

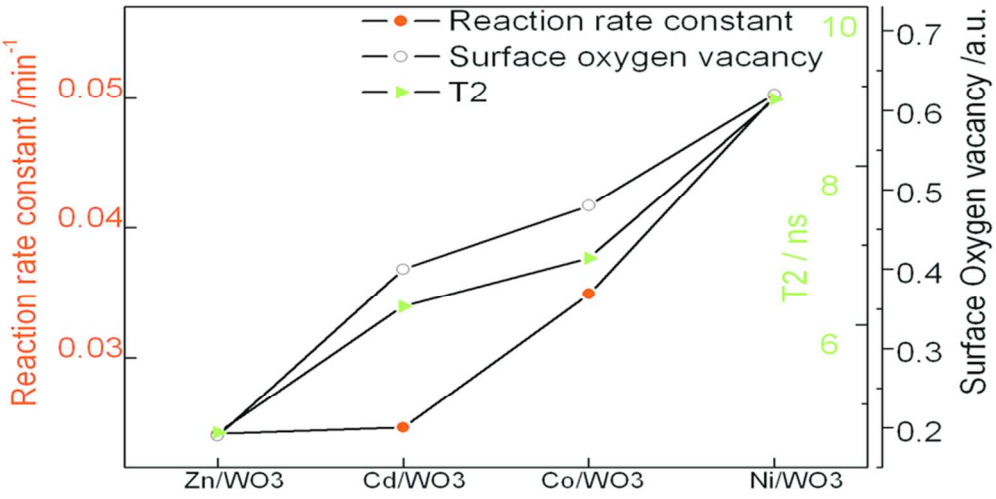

WO3 nanoplates derived from NiWO4 were found to have the highest ratio of WO3•2H2O, highest concentration of oxygen vacancy, narrowest band gap, longest electron-hole recombination time, and in turn the highest rate of photodegradation of Azo dye methylene blue.
80x39mm (300 x 300 DPI)

Journal Name

RSCPublishing

ARTICLE

Tuning the Electronic and Structural Properties of WO_3 Nanocrystals by Varying Transition Metal Tungstate Precursors

Cite this: DOI: 10.1039/x0xx00000x

Received ooth January 2012,
Accepted ooth January 2012

DOI: 10.1039/x0xx00000x

www.rsc.org/

Sara Rahimnejad[abc], Jing Hui He[ab], Wei Chen[* adb], Kai Wu[* eb], Guo Qin Xu *[ab]

Oxygen vacancy is one type of the most important defects affecting the photocatalytic performance of WO_3. In this paper, WO_3 nanoplates with high density of oxygen vacancies were synthesized from MWO_4 (M= Zn, Cd, Co, Ni) precursors using a sacrificial template method. The structures and morphologies of WO_3 nanoplates were investigated by field emission scanning electron microscopy (FE-SEM), high resolution Transmission Electron Microscopy (HRTEM), X-ray diffraction (XRD), X-ray photoelectron spectroscopy (XPS), Brunauer-Emmett-Teller (BET) analysis, Photoluminescence (PL), Diffuse Reflectance UV-Vis (DRS UV-Vis) and Time-correlated single-photon counting (TCSPC). The metal tungstates were found to not only act as the precursors but also as structure-directing agents during the growth of WO_3 nanoplates. XRD data revealed that two phases of $WO_3 \cdot xH_2O$ (x=1 or 2) were obtained after acid treatment of MWO_4. WO_3 nanoplates derived from $NiWO_4$ were found to have the highest ratio of $WO_3 \cdot 2H_2O$, highest concentration of oxygen vacancy, narrowest band gap, longest electron-hole recombination time, and in turn the highest rate of photodegradation of Azo dye methylene blue. These results show that the structural, electronic and photocatalytic properties of synthesized WO_3 nanoplates can be tuned by varying the transition metal tungstate precursors.

1. Introduction

Metal oxides have been widely studied due to their optical, magnetic, electronic and photocatalytic applications.[1-3] In particular, WO_3 is an important semiconductor material, which has been widely used in heterogeneous catalysis,[4,5] gas sensors,[6,7]electrochromic[8]/photochromic[9]/field emission[10,11] /solar energy devices[12] and photocatalysis.[13-22] Among these fields, the photocatalytic property was extensively investigated[23-27] due to its promising application for remediation of hazardous waste[28], water oxidation[29-31] and CO_2 reduction[32] because WO_3 has a high stability in acidic media[33], light-harvesting ability to visible light[34] and long-lasting energy storage ability.[35] However, the fast recombination rate of photogenerated electron (e^-)-hole (h^+) and rather low conduction band has inherently limited its photocatalytic effiency.[36] Several efforts were made to enhance the photocatalytic activity of WO_3 by tailoring its particle size,[37] crystal structure[38] and composition.[17] Recently, Yamakata et al. reported the relationship between the size of WO_3 particles and their photocatalytic efficiency.[37] Surprisingly, they discovered that large WO_3 particles with low surface area to volume ratios are suitable for photocatalytic oxygen evolution because of the long-lived photogenerated holes. This strongly suggest that shape and size of WO3 particles may not be the critical factor.

On the other hand, surface oxygen vacancies are intrinsic defects of metal oxides.[39] They are the most reactive sites on the surface and able to modify the electronic and chemical properties of the surface and greatly prolong life time of photoexcited carriers.[40] Therefore the amount of e^- and h^+ on the photocatalytic surface could be a key factor in determining the photocatalytic reaction rate.[41] Liu et al. also reported that the reactivity of a photocatalyst is mainly influenced by its surface geometric and electronic structures. Thus tuning the surfaces structures of WO_3 photocatalysts[41] to generate high-density e^- and h^+ is essential to optimize their photocatalytic performances for targeted reactions.[42] *Nowadays surface oxygen vacancy engineering is able to effectively enhance the photocatalytic performances of metal oxides.[43]*

Most of WO_3 nanocrystals were synthesized from aqueous solution of transition metal tungstates.[44,45] Many reports have confirmed the effects of preparation methods, the nature of supports[46-50]and tungsten precursors[51] on the

efficiency of WO_3 photocatalysts. However the influence of transition metal tungstate sources on fabricating WO_3 with different optical, electronic and photocatalytic properties has not been systematically studied yet. The present study aims to investigate the effects of precursors on the surface structures and photocatalytic behaviours of WO_3. The monoclinic WO_3 nanoplates with different densities of oxygen vacancies were prepared from transition metal tungstates MWO_4 (M= Zn, Cd, Co, Ni). Their photocatalytic efficiencies were evaluated by photo-degradation of methylene blue and are correlated with the changes of defects density in the samples prepared via varying the transition metal tungstate sources.

2. Experimental section

2.1 Chemicals and Materials

Tungsten oxide (WO_3 nanopowder, Sigma Aldrich), methylene blue (MB, Alfa-Aesar), nickel (II) nitrate hexahydrate 99.999%, zinc nitrate hexahydrate 99% (Sigma-Aldrich), sodium tungstate dehydrate 99% (Sigma-Aldrich), cadmium nitrate tetrahydrate (Sigma-Aldrich), cobalt (II) nitrate hexahydrate 99%, nitric acid 70% (Sigma-Aldrich) were used as received without further purification. Ultrapure deionized water was prepared by millipore purification system.

2.2 Preparation of MWO_4 (M= Zn, Cd, Co, Ni)

M $(NO_3)_2$ and Na_2WO_4 aqueous solutions with a molar ratio 1:1 were mixed at room temperature. The resulting precipitates were transferred into a Teflon-lined stainless steel autoclave at 160°C for 24 h. After hydrothermal treatment, the MWO_4 powders collected after filtration and washing with distilled water were dried in air at 80°C overnight.

2.3 Preparation of WO_3

The synthesized MWO_4 (M = Zn, Cd, Co, Ni) products from previous procedure were immersed in 8 mol·L^{-1} HNO_3 solution. The duration of acid treatment was varied from 24 h to 72 h depending on tungstate sources. Upon filtration and washing with distilled water, the acid treated products were calcined in a furnace at 500°C for 4 h in air.

2.4 Characterization

The morphology and microstructure of the samples were determined by SEM (JEOL-6701F) and TEM (JEM-3010). XRD patterns of the samples were recorded on a Panalytical X'pert XRD system using Cu Kα radiation. The optical absorbance spectra were recorded by a UV-visible spectrophotometer (Shimadzu UV-2600). The chemical state and valance band spectra of tungsten trioxides were characterized by X-ray photoelectron spectroscopy. Mg Kα (1253.6 eV) was utilized as the excitation light source and the signal was recorded by Omicron EA 125 at a normal emission angle at room temperature. The Brunauer–Emmett–Teller (BET) surface area was determined by nitrogen adsorption-desorption Isotherm measurement at 77 K using Micromeritics ASAP 2020. Photoluminescence (PL) Spectra were measured on a HORIBA Jobin Yvon S.A.S. Fluoromax-4 spectrofluorometer at an excitation wavelength of 320 nm. Fluroscence lifetime was measured on Flurolog HR 320 HORIBA Jobin Yvon S.A.S. time-correlated single photon counting (TCSPC) instrument.

2.5 Photocatalysis measurement

The photocatalytic activities of the prepared samples were evaluated by degradation of methylene blue under simulated solar light irradiation. In a typical run, 50 mg of photocatalysts was dispersed in 50 ml of Methylene blue aqueous solution (5mgL^{-1}). The solution was continuously stirred in the dark for 1 h to establish adsorption-desorption equilibrium before irradiation. The solution was then irradiated under illumination of a 500 W Xe lamp with light intensity of 100 mW/cm^2 was used as light source for simulated solar light. At each interval of 2 min, sample aliquots were exacted from the reactor, followed by centrifugation (13000 rpm for 5 min) and filtering through a 0.45 μm PTFE syring filter (Millipore) to remove the photocatalysts. The concentration of methylene blue was monitored by UV-Vis Spectrophotometer at the maximum absorbance peak (664 nm).

3. Result and discussion

3.1 Structure and Morphology

We first studied how the structures and compositions of WO_3 products are correlated with metal tungstate sources while keeping the other conditions constant. The XRD patterns of the uncalcined samples synthesized by different precursors are shown in Fig. 1. In the case of $ZnWO_4$, the acid treatment results in pure orthorhombic tungsten oxide hydrate $WO_3 \cdot H_2O$ phase (JCPDS No.43-0679) with lattice constants a = 0.5238 nm, b = 1.7040 nm, c = 0.5120 nm. The other three precursors (MWO_4, M = Cd, Co, Ni) result in $WO_3 \cdot 2H_2O$ phase (JCPDS No.16-0166) with lattice constants of a = 0.7450 nm, b = 0.6920 nm, c = 0.3720 nm mixed with $WO_3 \cdot H_2O$. This could be seen from the peak assignment marked by diamond and star symbols. Among these three precursors, $NiWO_4$ has the highest ratio of monoclinic $WO_3 \cdot 2H_2O$, which will correlate with the catalytic performance, as we will demonstrate later.

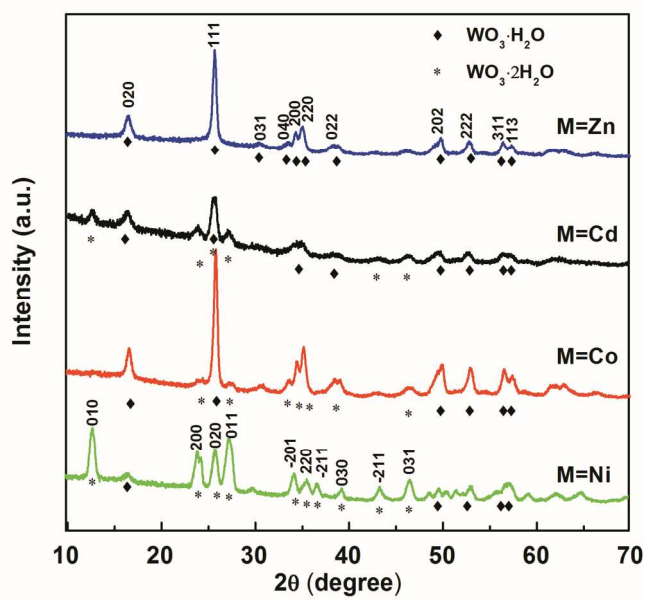

Fig. 1 X-ray diffraction (XRD) patterns of the $WO_3 \cdot xH_2O$ products synthesized by different precursors before calcination.

The above showed that both monoclinic $WO_3 \cdot 2H_2O$ and orthorhombic $WO_3 \cdot H_2O$ phases could be obtained by varying precursors. Further calcination at 500°C converts the crystal phase of these samples to pure monoclinic WO_3 (JCPDS No. 43-1035) as confirmed from the XRD results in Fig. 2. The normalized XRD peaks of the sample (Ni/WO_3) derived from $NiWO_4$ have the lowest intensities. This indicates a lower crystallinity, correlating to high oxygen-deficient surfaces.[52]

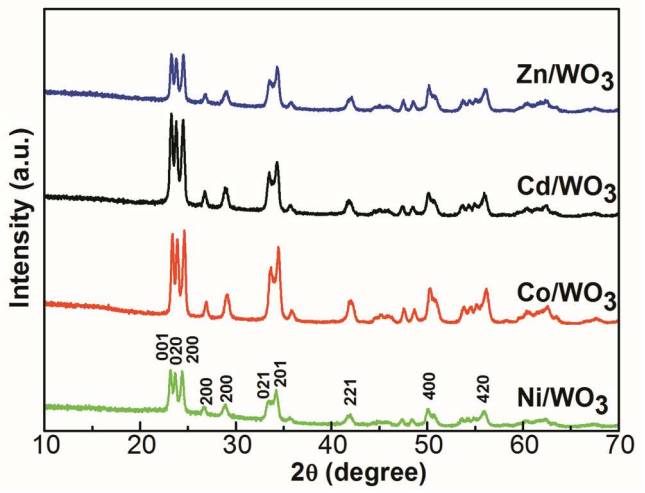

Fig. 2 X-ray diffraction (XRD) patterns of the products synthesized by different precursors after calcination.

Fig. 3 shows the representative FESEM images of WO_3 samples synthesized from different precursors. The result indicates that all products are of plate structure but the sizes of plates depend on precursors. In Fig. 3a, a typical plate is about 270 nm long and 220 nm wide. When the precursor was changed, the plates are of quasi-quadrangular shape (Fig. 3b-d). It is well proved that solvents, impurities and additives in solution can substantially influence the ultimate shape of the crystals by tuning the growth rate and orientation of the crystals.[53]This effect can be explained by different time duration for completing the process of replacing precursor cation by proton for each precursor, possibly affecting the rate of nucleation, growing, agglomeration and consequently ultimate shape.

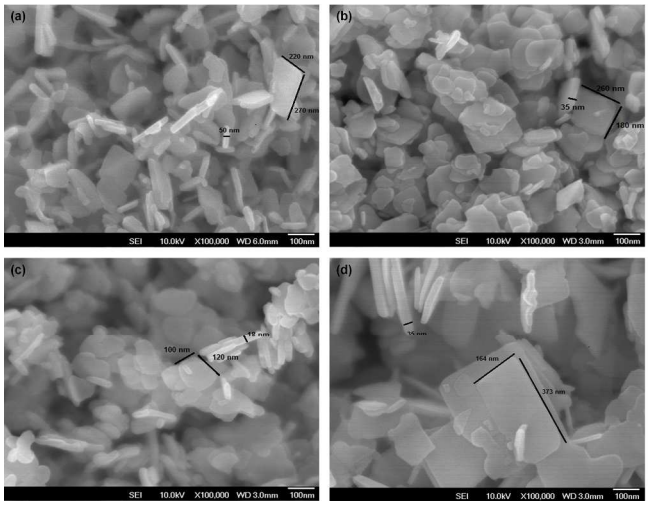

Fig. 3 Scanning electron microscopy (SEM) images of the products synthesized by different precursors: (a) Zn/WO_3 (b) Cd/WO_3 (c) Co/WO_3 (d) Ni/WO_3.

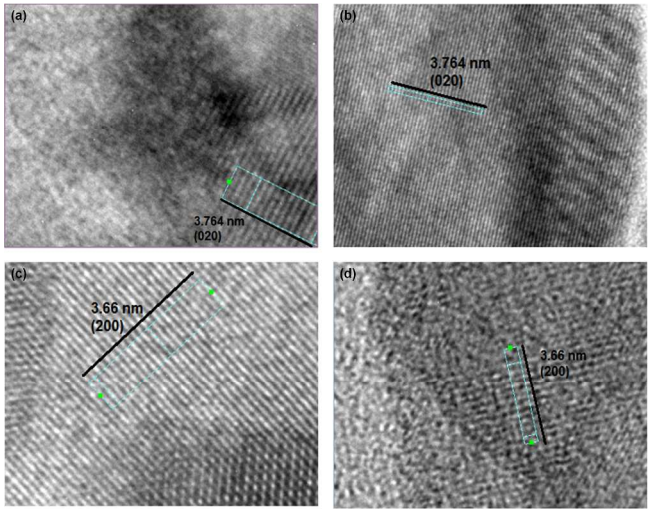

Fig. 4 HRTEM images of WO_3 samples by different precursors. (a) Zn/WO_3 (b) Cd/WO_3 (c) Co/WO_3 (d) Ni/WO_3.

The detailed structural and morphological characteristics of tungsten oxides were further investigated by HR-TEM. Fig. 4d shows that the synthesized Ni/WO_3 is not well crystallized. The HRTEM image shows the lattice fringes of 0.366 nm which can be readily assigned to (200) crystal planes. Fig. 4a-c show HR-TEM images of WO_3 derived from MWO_4 (M= Zn, Cd, Co). The result shows clear

crystal lattice, which can be assigned to the preferential orientation at (200) and (020) directions. Since (200) and (020) of WO_3 have equal surface energy and show the same adsorption ability[54], no correlation was observed between crystal facets of WO_3 and dye degradation.

BET surface area measurements of the samples were carried out at liquid nitrogen temperature, and the corresponding values are summarized in table 1. The specific surface area of the sample varies insignificantly, indicated that the WO_3 particle size was not crucial for photodegradation of azo dyes methylene blue.

Table 1 Comparison of Physical properties of different photocatalysts

Sample	BET Surface Area ($m^2 g^{-1}$)	BJH adsorption average pore diameter (nm)
Zn/WO_3	20.5	8.0
Cd/WO_3	17.8	8.3
Co/WO_3	15.2	8.1
Ni/WO_3	18.5	10.2

3.2. Electronic and Optical properties

To gain insight into the effect of different metal tungstates on the electronic and optical properties of WO_3 nanoplates, the chemical states and surface chemical compositions of the resultant crystals were determined by XPS. The O1s spectra of the WO_3 samples in Fig. 5 can be described as the superposition of three peaks located at 530.0, 531.2 and 533.0 eV. The O 1s peak at 533.0 eV indicates loosely bound oxygen, which is from H_2O molecules on the surface of WO_3. The peak at 530.0 eV is attributed to the O^{2-} ions mainly from bulk WO_3. The intensity at 531.2 eV is associated with O^{2-} in the oxygen deficient regions with the matrix of WO_3.[55] In the oxygen deficient surface region; OH^- groups are bonded to the metal cations to maintain the charge balance. Thus, the O 1s intensity of OH^- is related to the oxygen vacancy density. Since the concentration of lattice O^{2-} should not be sensitive to surface electronic structures; we normalize other peaks to this peak at 530.0 eV.[56] As Table 2 shows, the relative peak intensity at 531.2 eV of Ni/WO_3 is the highest among the four samples, correlating with the concentration of oxygen vacancies in WO_3 samples.

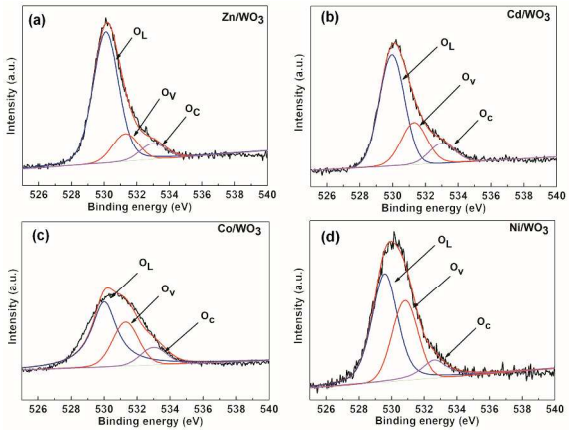

Fig. 5 XPS Spectra of the O $_{1S}$ region registered for WO_3 samples, fitted with three components, at 530.0, 531.2,533.0 eV for O^{2-}: O_L (lattice oxygen), OH^-: O_V (oxygen vacancy or defect), H_2O:Oc (chemisorbed oxygen species) respectively.

Table 2 O 1s signals for WO_3 based different precursors with the Relative Oxygen Species Amounts (The amounts of surface O^{2-}/OH^- /H_2O species were determined by XPS from the O1S peak (530.0, 531.3, 533.0 eV for O^{2-}, OH^-, H_2O respectively).

Peak Position (eV)	Zn/WO_3	Cd/WO_3	Co/WO_3	Ni/WO_3
530.0	1.0	1.0	1.0	1.0
531.3	0.19	0.40	0.48	0.62
533.0	0.11	0.19	0.18	0.19

To evaluate the effect of oxygen vacancy on the energy gap of the WO_3 samples prepared under different conditions, the optical properties of WO_3 samples were probed using UV-visible diffuse reflectance spectroscopy.

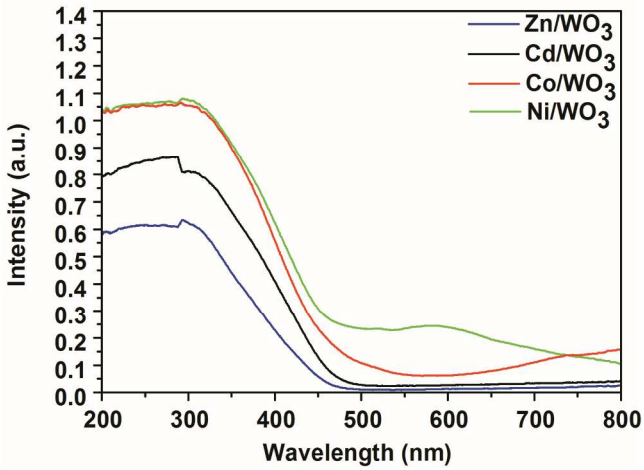

Fig. 6 Diffuse reflectance UV–vis of WO_3 samples obtained from different precursors.

The DR UV–vis spectra of WO_3 derived from MWO_4 (M= Zn, Cd, Co, Ni) are shown in Fig. 6. It could be found that

the optical absorption edge was estimated to be ~460 nm for WO_3 derived from $ZnWO_4$ and ~510 nm for WO_3 derived from $NiWO_4$, respectively. Combined with XPS results, with the increase of surface oxygen vacancy, the absorption edge of WO_3 gradually moved to longer wavelength.[55,57] We concluded that WO_3 derived from $NiWO_4$ has the highest O vacancy concentrations and thus the narrowest band gap as well as the best visible light response.

The relevant PL emission spectra and florescence life times of WO_3 samples were investigated and presented in Fig. 7 and 8. All samples have similar emission profiles. The blue emission peaks at 409 and 421 nm can be assigned to oxygen vacancies in WO_3.[58] The WO_3 sample derived from $NiWO_4$ has a significantly lower luminescence intensity compared to other WO_3 samples. Thus in this case we can observe the much lower PL intensity, which indicates the lower recombination rate of photo-induced electron-hole pair.

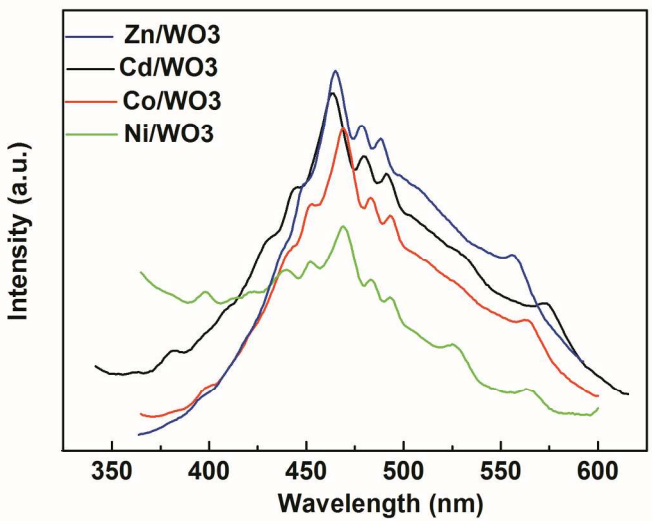

Fig. 7 PL spectra (using excitation at 340 nm) of WO_3 samples.

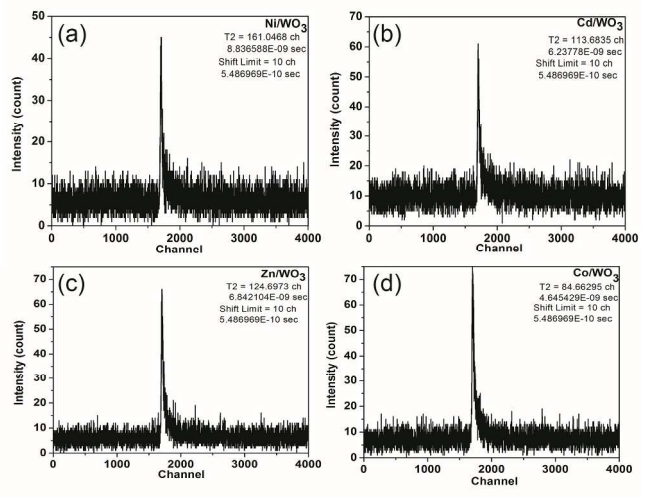

Fig. 8 Time-correlated single photon counting of fluorescence lifetimes of WO_3 samples.

Table 3 The calculated decay time constant for the commercial and as-prepared WO_3 samples

Sample	WO_3 commercial	Zn/WO_3	Cd/WO_3	Co/WO_3	Ni/WO_3
T2 (ns)	5.78	4.64	6.23	6.84	8.84

The much lower PL intensity indicates the lower recombination rate of photo-induced electron-hole pair and the presence of oxygen vacancies would facilitate the charge separation process. As reported, the oxygen vacancies are demonstrated to be electron donors in semiconductor[59] and can be considered to enhance the donor density in heterogeneous $WO_3 \cdot xH_2O/WO_3$ sample derived from $NiWO_4$.

The significant difference between the WO_3 samples is in the PL decay lifetime, as shown in Table 3. The PL decay of metal oxides comes from the recombination of nonradiative (T1) and radiative (T2) processes. The radiative process originates from the recombination of photogenerated electrons and holes. [60]Therefore we calculated the T2 values of different samples through double exponential decay fitting. The T2 values of as prepared are all greater than that of the commercial products (5.78 ns). In addition, Ni/WO_3 has the longest radiative decay time (8.84 ns). This longest lifetime corresponding to the slowest PL decay clearly shows a prolonged e^--h^+ recombination process.

Correlating with the formation mechanism of WO_3 samples, $WO_3 \cdot xH_2O$ was formed by the acid treatment and survived somehow after calcination. This facilitates the transfer of electrons to the surface of photocatalysts due to its highly conducting properties. Therefore the probability of photogenerated e-h^+ recombination decreases greatly by increasing the lifetime of photoexcited holes. On the other hand, the higher amount of O vacancies on the WO_3 sample from $WO_3 \cdot xH_2O$ which was formed after $NiWO_4$ acid treatment can increase the amount of charge carrier trapping sites on the surface which preventing the rate of e^--h^+ recombination and increase the life time of e^- and h^+ hole recombination.

The photocatalytic activities of resultant WO_3 crystals were evaluated by monitoring photodegradation of azo dye methylene blue. Among the WO_3 samples prepared from different precursors, the Ni/WO_3 exhibits the highest reaction rate; the rate constant is 5.01×10^{-2} min^{-1} as shown in Fig. 9. The rates constant were 3.49×10^{-2}, 2.46×10^{-2}, and 2.41×10^{-2} min^{-1} for other three samples. Correlating with Table 1, we found specific surface area is not the sole

determining factor. However, the photocatalytic degradation is a Pseudo First-order reaction judging from the good linearity of the curves in Fig. 9. The reaction rate constants were found to have the same trend as T2 values in PL spectra and the O1s peak intensity at 531.2 eV in XPS (Fig. 10) when the transition metal is varied from Zn to Cd, Co and Ni. Considering their physical meaning of T2 and 531.2 eV peak, this clearly demonstrates that the photoefficiency correlates with the e^--h^+ combination time and the concentration of surface oxygen vacancies.

The relation between the different metal sources and reaction rate constant may mainly come from the crystallographies of uncalcined samples. In the process of acid treatment on MWO_4 precursors, the hydrogen atoms exchange with lattice metal ions of MWO_4 crystals, forming $WO_3 \cdot xH_2O$ (x=1 or 2). Up on annealing these samples, the contained water molecules desorb and WO_3 nanoplates are formed. The crystalliferous water as in $WO_3 \cdot H_2O$ has weak interaction and is facile to release with no distortion on the WO_6 octahedrons during conversion to WO_3. Therefore the formed WO_3 nanoplates have less concentration of oxygen defects. In contrast, in $WO_3 \cdot 2H_2O$ (in fact $[WO_3\ (H_2O)] \cdot H_2O$)[61], there is one coordination water per W octahedron. This water molecule serves as a ligand, which is in fact part of the WO_6 octahedrons. Desorption of this coordinated water should leave a ligand defect, which will finally become an oxygen defect given no external oxygen atoms healing this vacancies during the formation of WO_3 nanoplates. The comparison between $WO_3 \cdot 2H_2O$ and $WO_3 \cdot H_2O$ will explain Zn/WO_3, which is from the pure $WO_3 \cdot H_2O$, has the lowest concentration of surface oxygen defects and thus the lowest photocatalytic efficiency and Ni/WO_3 is of the highest. Nevertheless, the uncalcined samples derived from Co, although of higher ratio of $WO_3 \cdot H_2O$ than that of Cd (Fig. 1) is unexpectedly of the higher oxygen vacancies. Therefore, other properties from the metal ions, rather than the sole crystallography, also play roles to control the oxygen vacancies, which are interesting in our future study.

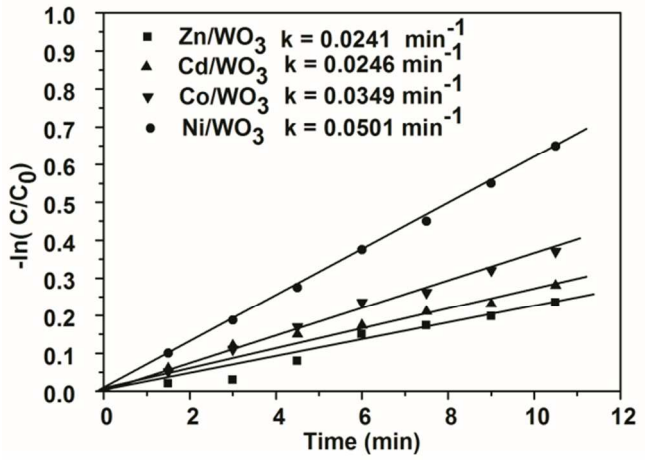

Fig. 9 Photocatalytic performance of methylene blue over WO_3 samples. The reaction rate constants (k) were calculated based on Pseudo-first order reaction kinetics. The light source was a 500 W Xenon lamp.

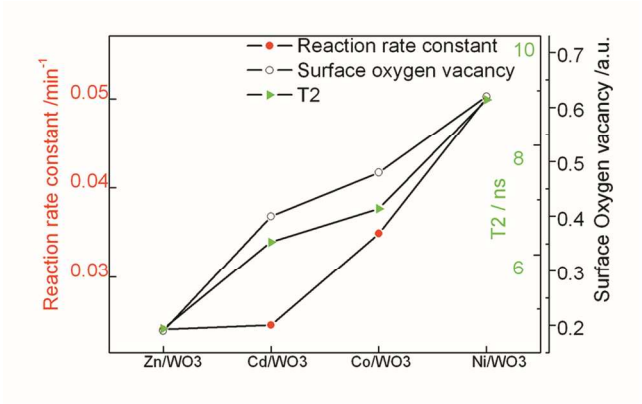

Fig. 10 Correlation of photoefficiency with the radiative time (T2) in PL process (Table 3) and concentration of surface oxygen vacancies from XPS O 1s peak at 531.3 eV (Table 1).

Conclusions

We have investigated the relationship between photocatalytic activities of WO_3 samples derived from different transition metal tungstate sources (M= Zn, Cd, Co, Ni) for dye degradation. We found that the concentration of oxygen vacancies of WO_3 sample generated from precursors is the decisive factor to the photocatalytic efficiency. The sample derived from $NiWO_4$ is of the highest ratio of OH^- to O^{2-}, longest PL lifetime decay and thus the highest photocatalytic efficiency. Our study may inspire the study of preparing precursors to optimize the photocatalytic efficiency of WO_3.

Acknowledgements

We are grateful for the financial support from the CREATE-SPURc project, National Research Foundation, Singapore (R143-001-205-592).

[a] Department of Chemistry, National University of Singapore, 3 Science Drive 3, 117543, Singapore. Email: chmxugq@nus.edu.sg Tel: +65 65163595
[b] SPURc, 1 CREATE Way, #15-01, CREATE Tower, Singapore 138602, Singapore
[c] Department of Chemistry, Yadegar-e-Imam Khomeini (RAH) Branch, Islamic Azad University,18155-144,Tehran,IRAN
[d] Department of Physics, National University of Singapore, 2 Science Drive 3, 117542, Singapore
[e] State Key Laboratory for Structural Chemistry of Unstable and Stable Species, College of Chemistry and Molecular Engineering, Peking University, Beijing, 100871, P. R. China

Notes and references

1 R.Ferrando, J.Jellinek and R.L. Johnston, *Chem.Rev.*, 2008, **108**, 845.
2 M. Ferna´ndez-Garcı´a, A. Martı´nez-Arias, J. C. Hanson and J. A. Rodriguez, *Chem. Rev.*, 2004, **104,** 4063.

3 D. V. Talapin, J.-S. Lee, M. V. Kovalenko and E. V. Shevchenko, *Chem. Rev.*, 2009, **110,** 389.
4 H.J. Liu, S.J. Huang, L. Zhang, S.L. Liu, W.J. Xin and L.Y. Xu, *Catal.Commun.*, 2009, **10,** 544.
5 D.H. Koo, M. Kim and S. Chang, *Org.Lett.*, 2005, **7,** 5015.
6 A. Ponzoni, E. Comini, G. Sberveglieri, J. Zhou, Sh. Zhi Deng, N.Sh Xu, Y. Ding and Zh.L. Wang, *Appl.Phys.Lett.*, 2006, **88**, 203101.
7 J. Ma, J. Zhang, Sh. Wang, T. Wang, J. Lian and X. Duan, *J.Phys.Chem.C*, 2011, **115**, 18157.
8 J.H. Zhu, S.Y. Wei, M. Alexander, T.D. Dang, T.C. Ho and Z.H. Guo, *Adv. Funct.Mater.*, 2010, **20**, 3076.
9 C.S. Blackman and I.P. Parkin, *Chem.Mater.*, 2005, **17**, 1583.
10 Y.B. Li, Y. Bando and D. Golberg, *Adv. Mater.*, 2003, **15,** 1294.
11 J.G. Liu, Z.J. Zhang, Y. Zhao, X. Su, S. Liu and E.G. Wang, *Small*, 2005, **1**, 310.
12 H.D. Zheng, Y. Tachibana and K. Kalantar-zadeh, *Langmuir*, 2010, **26**, 19148.
13 J. Shi, G. Hu, R. Cong, H. Bu and N. Dai, *New.J.Chem.*, 2013, **37**, 1538.
14 K. Sayama, H. Hayashi, T. Arai, M. Yanagida, T. Gunji and H. Sugihara, *Appl.Catal.B:Environ.,* 2010, **94**, 150.
15 D. Chen and J. Ye, *Adv.Funct.Mater.*, 2008, **18**, 1922.
16 Z.G. Zhao and M. Miyauchi, *Angew. Chem. Int. Edit.*, 2008, **47**, 7051.
17 I.M. Szilagyi, B. Forizs, O. Rosseler, A. Szegedi, P. Nemeth, P. Kiraly, G. Tarkanyi, B. Vajna, K. Varga-Josepovits, K. Laszlo, A.L.Toth, P.Baranyai and M.Leskela, *J.Catal.,* 2012, **294**, 119.
18 Y. Guo, X. Quan, N. Lu, H. Zhao and Sh. Chen, *Environ.Sci.Technol.*, 2007, **41**, 4422.
19 D. Sanchez-Martinez, A. Martinez-de la Cruz and E. Lopez-Cuellar, *Mater. Res. Bull.*, 2013, **48**, 691.
20 J. Huang, X. Xu, C. Gu, G. Fu, W. Wang and J. Liu, *Mater.Res.Bull.*2012, **47**, 3224.
21 S. Rajagopal, D. Nataraj, D. Mangalaraj, Y. Djaoued, J. Robichaud and O.Y. Khyzhun, *Nanoscale. Res. Lett.* 2009, **4**, 1335.
22 L. Zhang, X. Tang, Zh. Lu, Zh. Wang, L. Li and Y. Xiao, *Appl. Surf. Sci.* 2011, **258**, 1719.
23 Y. Liu, Q. Li, Sh. Gao and J. Ku Shang, *CrystEngComm.* 2014, **16**, 7493.
24 M. Mokhtar, S.A. Ahmed and Kh.S. Khairou, *Appl.Catal.B: Environ.* 2014, **150-151**, 63.
25 H. Zhang, J. Yang, D. Li, W. Guo, Q. Qin, L. Zhu and W. Zheng, *Appl. Surf. Sci.* 2014, **305**, 247
26 K. Jothivenkatachalam, S. Prabhu, A. Nithya and K. Jeganathan, *RSC.Adv.* 2014, **4**, 21221.
27 C. Gomez-Solis, D. Sanchez-Martinez, I. Juarez-Ramirez, A. Martinez-de la Cruz and L.M. Torres-Martinez, *J.Photoch.Photobio. A* 2013, **262**, 28.
28 M. Aslam, I.M.I. Ismail, S. Chandrasekaran and A. Hameed, *J.Hazmat.* 2014, **276**, 120.
29 G. Liu, J. Han, X. Zhou, L. Huang, F. Zhang, X. Wang, Ch. Ding, X. Zheng, H. Han and C. Li, . *J.Cat.* 2013, **307**, 148.
30 H. Ishihara, G.K. Kannarpady, Kh.R. Khedir, J. Woo, S. Trigwell and A.S. Biris, *Phys.Chem.Chem.Phys.* 2011, **13**, 19553.
31 K.C. Leonard, K.M. Nam, H.Ch. Lee, S.H. Kang, H.S. Park and A.J. Bard, *J.Phys.Chem.C* 2013, **117**, 15901.
32 X. Chen, Y. Zhou, Q. Liu, Zh. Li, J. Liu and Zh. Zou, *ACS Appl.Mater.Interfaces* 2012, **4**, 3372.
33 J.M. Spurgeon, J.M. Velazques and M.T. McDowell, *Phys.Chem.Chem.Phys.* 2014,**16**,3623.
34 A.J.E. Rettie, K.C. Klavetter, J.F. Lin, A. Dolocan, H. Celio, A. Ishiekwene, H.L. Bolton, K.N. Pearson, N.T. Hahn and C.B. Mmullins, *Chem.Mater.* 2014, **26**, 1670.
35 J. Li, Y. Liu, Zh. Zhu, G. Zhang, T. Zou, Zh. Zou, Sh. Zhang, D. Zeng and Ch. Xie, Sci.Rep. 2013, **3**, 2409; DOI: 10.1038/srep02409.
36 W. Gongming, L. Yichuan, W. Hanyu, Y. Xunyu, W. Changchun, Z. Zh. Jin and L. Yat, *Energy Environ.Sci.* 2012, **5**, 6180.
37 F. Amano, E. Ishinaga and A. Yamakata, *J.Phys.Chem.C* 2013, **117**, 22584.
38 M.R. Waller, T.K. Townsend, J. Zhao, E.M. Sabio, R.L. Chamousis, N.D. Browning and F.E. Osterloh, *Chem.Mater.*2012, **24,** 698.
39 W. Tu, Y. Zhou and Zh. Zou Adv. Mater. 2014, **26**, 4607.
40 P. Li, Y. Zhou, W. Tu, R.Wang, Ch.Zhang, Q.Liu, H. Li, Zh. Li, H. Dai, J. Wang, Sh. Yan and Zh. Zou, Cryst. Eng. Comm, 2013, **15**, 9855.
41 X.Y. Zhang, J. Qin, Y. Xue, P. Yu, B. Zhang, L. Wang and R. Liu, Sci.Rep. 2014, **4**, 4596; DOI:10.1038/srep04596.
42 Y.P. Xie, G. Liu, L. Yin and H.M. Cheng, *J.Mater.Chem.* 2012, **22**, 6746.
43 K.Xie, N.Umezawa, N. Zhang, P. Reunchan, Y. Zhang and J. Ye, Energy Environ. Sci., 2011, **4**, 4211.
44 Zh. Gu, T. Zhai, B. Gao, X. Sheng, Y. Wang, H. Fu, Y. Ma and J. Yao, *J.Phys.Chem. B* 2006, **110**, 23829.
45 A. Sonia, Y. Djaoued, B. Subramanian, R. Jacques, M. Eric, *Mater. Chem. Phys.*, 2012, **136**, 80.
46 J.M. Wang, E. Khoo, P.S. Lee and J. Ma, *J.Phys.Chem.C* 2008, **112**, 14306.
47 Zh. Wang, Sh. Zhou and L. Wu, *Adv. Funct. Mater.* 2007, **17**, 1790.
48 S. Rajagopal, D. Nataraj, D. Mangalaraj, Y. Djaoued, J. Robichaud and O.Y. Khyzhun, *Nanoscale. Res. Lett.* 2009**,** **4**, 1335.
49 X.Gao, Ch.Yang, F. Xiao, Y. Zhu, J. Wang and S. Xintai, *Mater. Lett.* 2012, **84**, 151.
50 L. Zhang, X. Tang, Zh. Lu, Zh. Wang, L.Li and Y. Xiao, *Appl. Surf. Sci.* 2011, **258**, 1719.
51 Y. Oaki and H. Imai, *Adv.Mater.*2006, **18**, 1807.
52 M. Lorenz, R. Bottcher, S. Friedlander, A. Poppl, D. Spemann, *J. Mater. Chem. C*, 2014, **2**, 4947.
53 G. Liu, J.C. Yu, G.Q. Lu, H.M. Cheng, *Chem. Commun.*, 2011, **47**, 6763.
54 D. Zhang, S. Wang, J. Zhu, H. Li, Y. Lu, *Appl. Catal., B.* 2012, **123-124**, 398.
55 J. Wang, Z. Wang, B. Huang, Y. Ma, Y. Liu, X. Qin, X. Zhang and Y. Dai, *ACS Appl. Mater. Interfaces* 2012, **4**, 4024.
56 G. Wang, Y. Ling, H. Wang, X. Yang, Ch. Wang, J.Z. Zhang and Y. Li, *Energy Environ.Sci.* 2012, **5**, 6180.
57 J. Cao, B. Luo, H. Lin, B. Xu, Sh. Chen, *Appl.Catal.B:Environ.* 2012, **111-112**, 288.
58 W. Hu, Y. Zhao, Z. Liu, C.W. Dunnill, D.H. Gregory and Y. Zhu, *Chem.Mater.* 2008, **20**, 5657.
59 Y.Y. Tay, T.T. Tan, M.H. Liang, F. Boey and S. Li, *Phys.chem.chem.phys*. 2010, **12**, 6008.

60 F. Wang, X. Chen, X. Hu, K.S. Wong and J.C. Yu, *Sep. Purif. Technol*. 2012, **91**, 67.
61 J.A. Kaduk, *Powder Diffr*. 2008, **23**, 157-158.

